DOI: 10.1002/ejic.201100132

Syntheses, Structures, and Properties of Trinuclear Copper(I)/Titanium(IV) Thiolate Complexes

Vasyl Andrushko,[a] Heino Sommer,[a] Daniel Himmel,[b] Dieter Fenske,[a,c] and Andreas Eichhöfer*[c]

Keywords: Copper / Titanium / Sulfur / Cluster compounds / Density functional calculations

The thiolato-bridged copper(I)/titanium(IV) complexes $[Li(15\text{-crown-}5)thf]_2[Cu_2Ti(SPh)_8]$ (thf = tetrahydrofuran) and $[Cu_2Ti(SPh)_6(PPh_3)_2]$ have both been prepared in yields of at least 83 % by reaction of CuCl and $TiCl_4{\cdot}2thf$ with LiSPh in THF in the presence of 15-crown-5 or PPh_3, respectively. The crystal structures of the trinuclear compounds were determined by X-ray analysis of single crystals. The dark colored compounds display absorption bands over a wide energy range with absorption onsets lying in the near infrared region at approximately 1350 nm for $[Li(15\text{-crown-}5)thf]_2[Cu_2Ti(SPh)_8]$ and 1050 nm for $[Cu_2Ti(SPh)_6(PPh_3)_2]$. Density functional calculations reproduce and explain the energy difference of the lowest energy transitions. Thermal treatment of $[Cu_2Ti(SPh)_6(PPh_3)_2]$ up to 500 °C resulted in the cleavage of SPh_2 and PPh_3 and the formation of a mixture of ternary copper titanium sulfides, namely Cu_4TiS_4 and the defect thiospinel $Cu_{0.33}TiS_2$. In contrast, reflections of the powder diffraction patterns of the residues from the thermal analysis of $[Li(15\text{-crown-}5)thf]_2[Cu_2Ti(SPh)_8]$ could only be assigned to the known phases $Cu_{1.8}S$ (Digenite) and $Cu_{1.96}S$ (Djurleit).

Introduction

In recent years early transition-metal thiolate complexes have received attention because of their importance in a wide range of areas.[1] Interest in titanium thiolate compounds arises from the fact that such compounds can serve as single-source precursors for the formation of thin films of titanium sulfides by chemical vapor deposition (CVD).[2,3–8] Titanium disulfide is also of interest since Whittingham first demonstrated fast, reversible Li insertion into TiS_2 over the solid solution range $0 \leq x \leq 1$ of Li_xTiS_2.[9,10] However, only a few homoleptic titanium complexes with monodentate thiolato ligands have been characterized by single-crystal X-ray to date. Examples include $[Li(OEt_2)_3][Ti(S\text{-}2,4,6\text{-}iPr_3C_6H_2)_4]$,[11] $[NMe_2H_2][Ti_2(SMe)_9]$, $[Ti_3(SMe)_{12}]$,[12] $[Ti\{S\text{-}1,3,4,6\text{-}C_6H(CH_3)_4\}_4]$,[13] $[NEt_4]_2[Ti(SPh)_6]$,[14] $[Li(C_4H_8O)_4][Ti_2(SPh)_9]$,[15] $[NH_2Et_2]_2[Ti_2(SCH_2Ph)_9]$,[7] and $[NH_2Et_2]_2[Ti(SC_6F_5)_6]$, some of them isolated only in low yields.[8]

Interest in the combination of an early and a late transition metal in a heterobimetallic complex arises because the combination of two different metal atoms, which are electron-deficient and electron-rich, respectively, offers the possibility of Lewis acid activation of a substrate molecule bound to the electron-rich metal center. Thiolato-bridged titanium heterometallic compounds have been featured in reviews over the last two decades.[1,16,17] It is noteworthy that bimetallic complexes, such as $[Cp_2Ti(\mu\text{-}SCH_2CH_2CH_3\text{-}PPh_2)_2Rh]BF_4$, reveal reversible Ti^{IV}/Ti^{III} redox couples,[18] whereas the corresponding metalloligands do not. In addition, it was suggested that relatively short Ti–Cu distances of 280.3 pm in $[Cp_2Ti(SCH_2CH_3)_2CuP(C_6H_{11})_3]PF_6$[19] and 280.93 to 283.2 pm in $[Cp_2Ti_2Cu_2(\mu_3\text{-}S)_4(PPh_3)_2]$[20] are consistent with $Cu(d^{10}) \rightarrow Ti(d^0)$ dative interactions. However, recent investigations by our group on the cluster complexes $[Li(THF)_4]_2[Ti_2Cu_8S_4(SPh)_{10}]$ and $[Ti_2Ag_6S_6Cl_2(PPhiPr_2)_6]$ do not provide any support for $d^{10} \rightarrow d^0$ dative bonding in these compounds.[21] Related solid state materials, such as $CuTi_2S_4$, have recently attracted interest as cathode materials in rechargeable lithium ion batteries[22,23] supported by first principles total energy calculations on the intercalation of copper into TiS_2, which significantly influences its electronic properties.[24]

Here we report the syntheses and crystal structures of the mixed titanium(IV)/copper(I) trinuclear thiolate complexes $[Li(15\text{-crown-}5)thf]_2[Cu_2Ti(SPh)_8]$ (**1**) and $[Cu_2Ti(SPh)_6(PPh_3)_2]$ (**2**) along with investigations on their optical and thermal properties.

[a] Institut für Anorganische Chemie, Karlsruher Institut für Technologie (KIT), Campus Süd,
Engesserstr. 15, 76131 Karlsruhe, Germany
[b] Institut für Anorganische und Analytische Chemie, Albert-Ludwigs-Universität Freiburg,
Albertstr. 21, 79104 Freiburg, Germany
[c] Institut für Nanotechnologie, Karlsruher Institut für Technologie (KIT), Campus Nord,
Hermann-von-Helmholtz-Platz 1, 76344 Eggenstein-Leopoldshafen, Germany
Fax: +49-721-608-26368
E-mail: andreas.eichhoefer@kit.edu
Supporting information for this article is available on the WWW under http://dx.doi.org/10.1002/ejic.201100132.

Results and Discussion

Synthesis and Structure

Both mixed titanium(IV)/copper(I) trinuclear thiolate complexes **1** and **2** were prepared by the reaction of CuCl and $TiCl_4$·2thf with LiSPh in THF at room temperature (Scheme 1). Addition of either two eq. of 15-crown-5 at –15 °C or two eq. of PPh_3 at room temp. to the dark lilac reaction mixtures afforded the crystallization of almost black crystals of **1** and **2**.

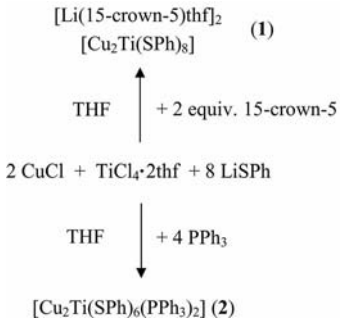

Scheme 1.

Ionic **1** crystallizes in the monoclinic space group $P2_1/n$ (Table 2). The molecular structure of the cluster anion $[Cu_2Ti(SPh)_8]^{2-}$ in **1** is shown in Figure 1. There is an inversion center at the titanium atom, and **1** can be viewed as consisting of a distorted octahedral titanium atom sharing parallel trigonal faces with two copper [Cu(1) and Cu(1′)] centred tetrahedra. Six of the thiolato ligands [S(1)–S(3) and symmetry equivalent positions] act as μ_2-bridges [Cu–S–Ti: 70.24–70.83(2)°] at the corners of the shared faces, and two others [S(4) and S(4)′] act as terminal ligands coordinated to the copper atoms. The Ti–S bond lengths [245.57–248.13(8) pm] are shorter than those found in octahedral $[Ti(SPh)_6]^{2-}$[14] [255.3–258.5(3) pm] and in between the values found for $[Ti_2(SPh)_9]^-$[15] [232.40–254.34(17) pm], whereas the Cu–S distances [μ_2-SPh–Cu: 234.38–236.42(7) pm, μ_1-SPh–Cu: 223.13(7) pm] are slightly longer than those found in $[Cu_4(SPh)_6]^{2-}$ (Cu–S: 224.5–230.6 pm).[25] Whereas the octahedral thiolate coordination around titanium is only moderately distorted [S–Ti–S: 86.74–93.26(2)°], the copper center sits in a strongly distorted tetrahedral environment [S–Cu–S: 91.67–130.44(3)°]. The copper–titanium distance [Cu···Ti: 278.78(5) pm] is comparable to those found in $[Cp_2Ti(SCH_2CH_3)_2CuP(C_6H_{11})_3]PF_6$[19] (Cu···Ti: 280.3 pm) and $[Ti_2Cu_2S_4Cp_2(PPh_3)_2]$[20] (Cu···Ti: 280.93–283.2 pm), which were attributed to Cu(d^{10})→Ti(d^0) dative bonding interactions. Recent investigations on $[Ti_2Cu_8S_4(SPh)_{10}]^{2-}$ (Cu···Ti: 277.7–278.8 pm),[21] however, suggest that there is no evidence for d^{10}→d^0 dative bonding interactions in these compounds.

Complex **2** crystallises in the trigonal space group *R*3 (Table 2). The trinuclear unit "$Cu_2Ti(SPh)_6$" with six μ_2-bridging thiolato ligands is structurally similar to that observed in the anion of **1**, and the terminal SPh^- groups are replaced by two coordinating triphenylphosphane molecules resulting in a neutral molecule (Figure 2). A threefold rotation axis runs through the linear chain formed by the copper titanium and phosphorus atoms P(1)–Cu(1)···Ti(1)···Cu(2)–P(2) (Figure 2). Considering only the heavy element framework in **2**, there is a nearly pseudo inversion symmetry center at the titanium atom, which is not valid for the disordered phenyl rings (see Exp. Section). The geometric parameters compare with those observed in the anion of **1** with a similar range of octahedral S–Ti–S angles in **1** [86.74–93.26(2)°] and **2** [86.40–93.23(13)°]. Mean μ_2-S–

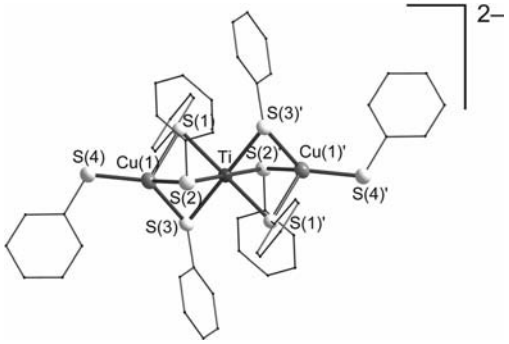

Figure 1. Molecular structure of the cluster anion $[Cu_2Ti(SPh)_8]^{2-}$ in the crystal of **1** (50% ellipsoids, H atoms omitted for clarity). Symmetry transformation for generation of equivalent atoms: ′ $–x – 1, –y, –z + 2$. Selected bond length [pm]: Ti(1)–S(1) 246.40(9), Ti(1)–S(2) 248.13(8), Ti(1)–S(3) 245.57(7), Cu(1)–S(4) 223.13(7), Cu(1)–S(1) 234.38(7), Cu(1)–S(2) 236.18(7), Cu(1)–S(3) 236.42(7), Ti(1)···Cu(1) 278.78(5), Selected bond angles [°]: Cu(1)–Ti(1)–Cu(1)′ 180.0, S(4)–Cu(1)–Ti(1) 167.80(2), S(3)–Ti(1)–S(1) 88.45(2), S(3)′–Ti(1)–S(1) 91.55 (2), S(3)′–Ti(1)–S(2)′ 86.74(2), S(1)–Ti(1)–S(2) 86.80(2), S(3)–Ti(1)–S(2)′ 93.26(2), S(1)–Ti(1)–S(2)′ 93.20(2), S(4)–Cu(1)–S(1) 111.40(3), S(4)–Cu(1)–S(2) 130.44(3), S(1)–Cu(1)–S(2) 92.41(3), S(4)–Cu(1)–S(3) 127.33(3), S(1)–Cu(1)–S(3) 93.58(3), S(2)–Cu(1)–S(3) 91.67(3), Cu(1)–S(1)–Ti(1) 70.83(2), Cu(1)–S(2)–Ti(1) 70.24(2), Cu(1)–S(3)–Ti(1) 70.65(2).

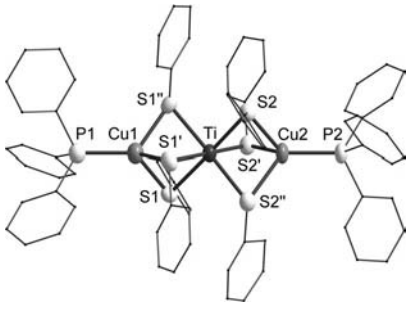

Figure 2. Molecular structure of **2** in the crystal viewed down *a* (50% ellipsoids, disordered C atoms and all H atoms omitted for clarity). Symmetry transformation for generation of equivalent atoms: ′ $–y + 1, x – y, z$; ′′ $–x + y + 1, –x + 1, z$. Selected bond length [pm]: Cu(1)–P(1) 220.4(5), Cu(1)–S(1) 234.6(3), Cu(2)–P(2) 225.0(5), Cu(2)–S(2) 235.4(4), Ti(1)–S(2) 242.8(4), Ti(1)–S(1) 248.6(4), Cu(1)···Ti(1) 280.4(5), Cu(2)···Ti(1) 276.2(5), Selected bond angles [°]: P(1)–Cu(1)–Ti(1) 180.0, P(2)–Cu(2)–Ti(1) 180.0, Cu(2)–Ti(1)–Cu(1) 180.0, P(1)–Cu(1)–S(1) 123.10(7), S(1′)–Cu(1)–S(1) 93.01(10), P(2)–Cu(2)–S(2) 124.02(8), S(2)–Cu(2)–S(2′) 91.75(11), Cu(1)–S(1)–Ti(1) 70.88(12), Cu(2)–S(2)–Ti(1) 70.54(13), S(2)–Ti(1)–S(1) 178.53(18), S(2)–Ti(1)–S(2′) 88.21(15), S(2)′–Ti(1)–S(1) 93.23(12), S(2)–Ti(1)–S(1′) 92.15(11), S(1)–Ti(1)–S(1′) 86.40(13), Cu(1)–S(1)–Ti(1) 70.88(12), Cu(2)–S(2)–Ti(1) 70.54(13).

Ti distances were found to be 246.7 pm in **1** and 245.7 pm in **2**, and mean μ_2-S–Cu distances are 235.7 in **1** and 235.0 pm in **2**.

A similar linear metal skeleton has been observed in some heterobimetallic trinuclear complexes such as $[Cu_2M(SAr)_6(PPh_3)_2]$ (M = W, Mo, U; Ar = Ph, *p*-C_6H_4Me, *p*-C_6H_4F, *p*-C_6H_4Cl, *p*-C_6H_4Br),[26–28] $[Cu_2Sn(SPh)_6(PPh_3)_2]$,[29] and $[LFeMFeL]^{n+}$ [M = Ge, Sn; *n* = 2, 3; L = 1,4,7-(4-*tert*-butyl-2-mercaptobenzyl)-1,4,7-triazacyclononane].[30]

A comparison of the measured and calculated X-ray powder diffraction patterns for **1** and **2** reveals the crystalline purity of **2** with respect to the formation of other crystalline compounds (Figure 3). Slightly increasing differences in the position of the peaks with increasing detection angle arises from the temperature difference of the detection of the single crystal data and the powder patterns. Visible deviations of the measured and simulated powder patterns of **1** could be attributed to a loss of solvent molecules, although the samples were measured as a suspension in THF.

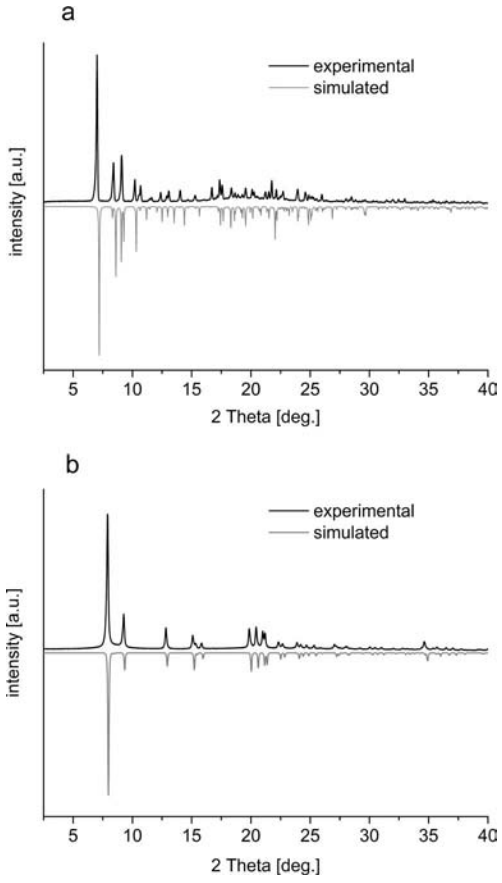

Figure 3. Powder diffraction pattern of a) **1** as a suspension of crystals in THF and b) **2** as a dried crystalline powder.

Electronic Spectra

UV/Vis spectra of the crystalline powders of **1** and **2** were measured as a nujol mull pressed between quartz plates (Figure 4). Due to the decomposition of **1** and insolubility of **2** in organic solvents no solution spectra were measured. In accordance with the dark color of the mulls (**1** dark green; **2** grey–blue) both compounds show several absorption features which cover the whole visible region and reach into the near infrared. Differences between the spectra of both compounds are a) the tail of the absorption onset which is observed in **1** further into the infrared at 1350 nm than in **2** (1050 nm), b) the first two maxima are shifted to smaller wavelengths on going from **1** (912, 665 nm) to **2** (875, 633 nm), c) an additional absorption maximum at 511 nm in **2**, and d) another shifted maximum (shoulder) [**1**: 406 and **2**: 373(sh) nm].

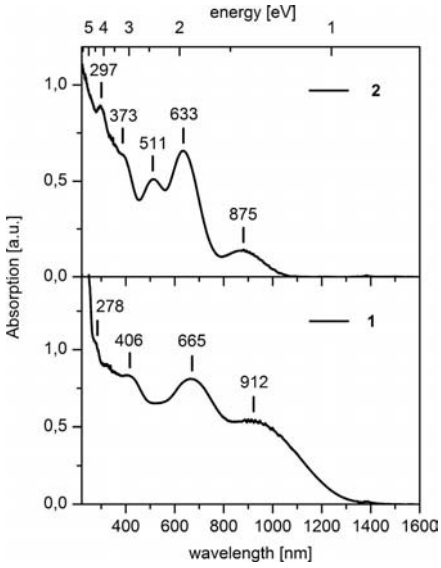

Figure 4. UV/Vis spectra of **1** and **2** in the solid state (powder in mineral oil between quartz plates).

Absorption features at wavelengths below 300 nm [**1**: 278 (sh); **2**: 297 nm] can be assigned to π–π* transitions of the SPh^- and PPh_3 ligands.[31] As copper thiolato complexes such as $(NEt_4)_2[Cu(SPh)_3]$,[31] $(NEt_4)_4[Cu_6(SPh)_4Cl_6]$,[32] and $(PPh_4)_2[Cu_4\{o\text{-}(SCH_2)_2C_6H_4\}_3]$[33] are known to form white to light orange compounds with absorption features below 320 nm, we suggest that most of the other transitions in **1** and **2** are mainly assigned to LMCT transitions from SPh^- into low lying empty *d* orbitals of Ti^{4+}. For orange red $[Ti(SCH_2CH_2S)_3]^{2-}$ where titanium is coordinated by six sulfur atoms in a distorted octahedron, Holm reported "a rich LMCT" spectrum in CH_3CN with absorption features from 550 to 200 nm [230, 276 (sh), 355, 414, 476 (sh)].[34] Other thiolato complexes of six-coordinate titanium atoms such as $[NMe_2H_2][Ti_2(SMe)_9]$, $[Ti_3(SMe)_{12}]$,[12] $[NEt_4]_2[Ti(SPh)_6]$,[14] $[Li(C_4H_8O)_4][Ti_2(SPh)_9]$,[15] $[NH_2Et_2]_2[Ti_2(SCH_2Ph)_9]$,[7] and $[NH_2Et_2]_2[Ti(SC_6F_5)_6]$[7] are reported to form deep colored dark red to black crystals but no electronic absorption data are given. However, the differences between the spectra of ionic **1** and neutral **2** upon formal exchange of two SPh^- ligands with two PPh_3 ligands indicate the involvement of transitions from copper based *d* orbitals as the distorted octahedral coordination environment around the titanium atoms does not change in either com-

pound but the copper coordination environment does. Furthermore, it has been suggested that low energy bands at around 650 nm in copper titanium thiolato complexes such as $[Cp_2Ti(\mu_2\text{-}SCH_3)_2CuX]_n$ (X = Cl, Br), which have not been characterized by single crystal XRD, are attributable to transitions involving both metal centers.[35] Instead, in thf solutions of crystallographically characterized $[Cp_2Ti(\mu_2\text{-}SCH_2CH_3)_2CuP(C_6H_{11})_3]PF_6$ only two absorption bands at 462 and 354 nm were found with no evidence for MMCT transitions.[19]

In order to characterize the nature of the optical transitions more carefully, density functional calculations at the BP86[36,37]/SV(P)[38] level of theory were performed on the dianion in **1** and on **2**. It must be noted that the optimised gas phase structures differ significantly in both cases from the crystal structures (Table 4 and Figure S7 and S8 in the Supporting Information). During optimisation, the dianion in **1** undergoes a drastic change to a very asymmetric structure with one three-coordinate copper atom, whereas the symmetry of **2** increases from point group C_3 to S_6 making many transitions Laporte forbidden due to the inversion center in S_6. Thus, for the quantum chemical considerations, only the H atom positions were kept in their crystal framework. The

Table 1. The ten lowest calculated transition energies [nm] and their oscillator strengths f_{osc} in **1c** and **2c**.

	1c		**2c**	
No.	λ [nm]	f_{osc}	λ [nm]	f_{osc}
1	1617	1.5×10^{-3}	1069	2.8×10^{-3}[a]
2	1471	2.0×10^{-2}	852	1.3×10^{-4}
3	1459	–[b]	812	6.0×10^{-3}[a]
4	1238	2.0×10^{-3}	780	7.7×10^{-4}
5	1211	2.0×10^{-3}	729	5.6×10^{-5}[a]
6	1260	–[b]	693	8.0×10^{-4}[a]
7	909	3.1×10^{-3}	676	5.1×10^{-3}
8	883	3.1×10^{-3}	648	3.1×10^{-2}
9	853	4.5×10^{-3}	630	1.6×10^{-3}[a]
10	824	–[b]	625	2.4×10^{-3}[a]

[a] Degenerate transition. [b] Laporte forbidden.

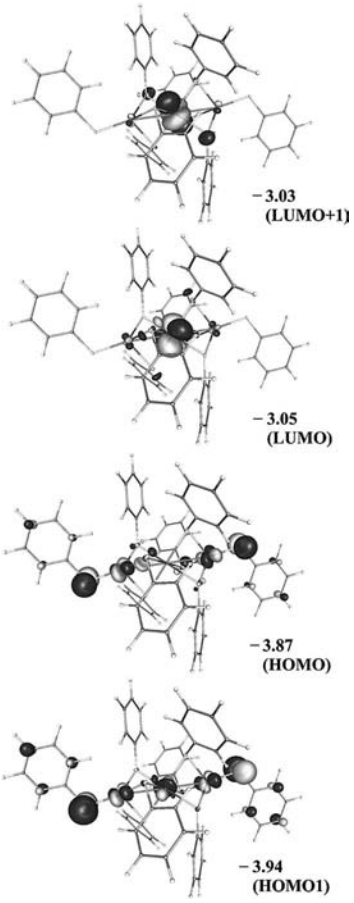

Figure 5. Molecular frontier orbitals of **1c**. Contours are drawn at 0.05 a.u., orbital energies (right) are given in eV.

Table 2. MO contributions (%) in the frontier orbitals of **1c**.

MO No.	265 HOMO–3	266 HOMO–2	267 HOMO–1	**268 HOMO**	**269 LUMO**	270 LUMO+1	271 LUMO+2	272 LUMO+3
E [eV]	–4.38	–4.06	–3.94	**–3.87**	**–3.05**	–3.03	–2.41	–1.55
Σ Cu	53	37	29	**34**	**3**	3	11	1
Ti	1	0	7	**0**	**76**	77	67	36
Σ μ-S	35	32	11	**17**	**14**	14	15	10
Σ term. S	2	20	34	**31**	**0**	0	3	0
Σ phenyl[a]	10	11	19	**18**	**6**	7	4	54

[a] Contains small unassigned contributions from AOs (< 0.1%) of Cu, Ti and S.

Table 3. MO contributions (%) in the frontier orbitals of **2c**.

MO No.	343 HOMO–3	344+345 HOMO–2	346+347 HOMO–1	**348 HOMO**	**349+350 LUMO**	351 LUMO+1	352+353 LUMO+2	354+355 LUMO+3
E [eV]	–5.49	–5.24	–5.03	**–4.69**	**–3.54**	–3.01	–1.93	–1.88
Σ Cu	27	37	42	**26**	**2**	9	1	1
Ti	11	7	2	**0**	**78**	68	28	4
Σ μ-S	16	38	44	**45**	**14**	16	9	2
Σ P	8	1	1	**9**	**0**	3	2	8
Σ phenyl[a]	39	18	11	**21**	**6**	5	61	85

[a] Contains small unassigned contributions from AOs (< 0.1%) of Cu, Ti, S and P.

structures obtained are denoted as **1c** and **2c** (Table S3 and S4 in the Supporting Information). Crystal lattice effects were simulated with COSMO[39] screening charges, which was crucial for the dianion to shift the Kohn–Sham orbital energies to physically meaningful negative values.

In accordance with the observed redshifted lowest energy absorption of **1** in comparison with **2**, **1c** exhibits a smaller HOMO–LUMO gap (0.82 eV) than **2c** (1.15 eV). Time-dependent DFT calculations yield systematically lower transition energies in **1c** compared to **2c**. The ten lowest calculated transition energies are given in Table 1 (see also Table S1 and S2 in the Supporting Information). A Mullikan population analysis[40] of the orbitals that contribute to the lowest energy transitions reveals common features in both complexes. Summarised MO contributions are given in Tables 2 and 3 and the respective orbitals are visualised in Figure 5 (see also tables S5 and S6 in the Supporting Information). All the transitions in Table 1 are from orbitals that are delocalised mainly over the copper and sulfur atoms into orbitals which are essentially localised at the titanium atoms. The main effect of the exchange of a terminal thiolato ligand in **1c** with the phosphane ligand in **2c** can be explained as follows: although in **2c** the contribution of the phosphane ligands to the HOMO and HOMO–1 can almost be neglected, the terminal thiolato ligand contribution in **1c** is in the same magnitude as that of one of the copper atoms. The antibinding π donor interaction of the lone pair *p* orbitals at the terminal sulfur atoms with *d* orbitals at the copper atoms increases the orbital energies of the HOMO and HOMO–1 in **1c** and reduces the transition energies (Figure 6).

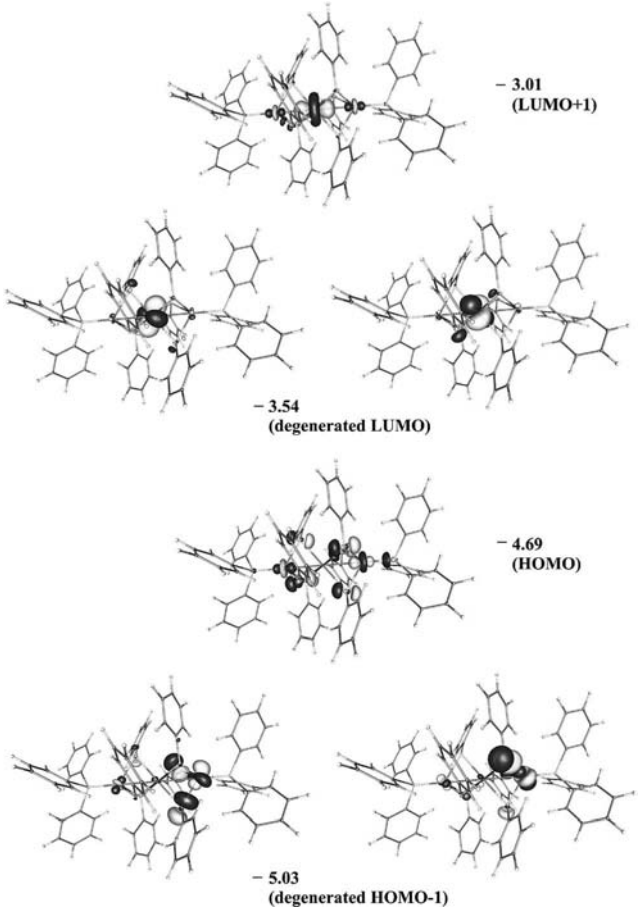

Figure 6. Molecular frontier orbitals of **2c**. Contours are drawn at 0.05 a.u., orbital energies (right) are given in eV.

Thermal Behavior

Concerning the use of titanium thiolato complexes in CVD processes, Bochmann et al. reported that heating the volatile titanium thiolate $Ti(StBu)_4$ to 130–200 °C under vacuum leads to the deposition of amorphous films of TiS.[3] Thiol adducts of the type $[TiCl_4(HSR)_2]$ (R = *c*-C_6H_{11} or *c*-C_5H_9) were found to afford bronze colored films of polycrystalline TiS_2 in CVD experiments (200–600 °C, at 0.1 Torr).[4,5] Girolami et al. observed that passing $Ti(StBu)_4$ over quartz, silicon, and stainless steel substrates at temperatures of 150 and 270 °C and 10^{-4} Torr resulted in the deposition of grey–blue films of TiS_2.[6] Recently, Carmalt et al. reported low pressure CVD experiments using $[NH_2Et_2]_2[Ti_2(SCH_2Ph)_9]$[7] and $[NH_2Et_2]_2[Ti(SC_6F_5)_6]$,[8] which led to the formation of films of TiS_2. Thermal decomposition experiments on heteronuclear copper titanium thiolato complexes have not been reported so far.

Thermogravimetric analysis of **1** under a helium gas flow shows that it starts to decompose above 30 °C in a two step process (1st step: 30–90 °C; 2nd step: 90–350 °C), whereas **2** displays a one step mass loss ranging from 80 °C to 370 °C with an additional minor mass loss in the region from 370 to 475 °C. (Figure 7). Both total mass losses (**1** 79.5; **2** 81.6%) are close to those required for complete decomposition of **1** to form $Li_2Cu_2TiS_4$ (calcd. 80.8%) and **2** to form Cu_2TiS_3 (calcd. 80.0%).

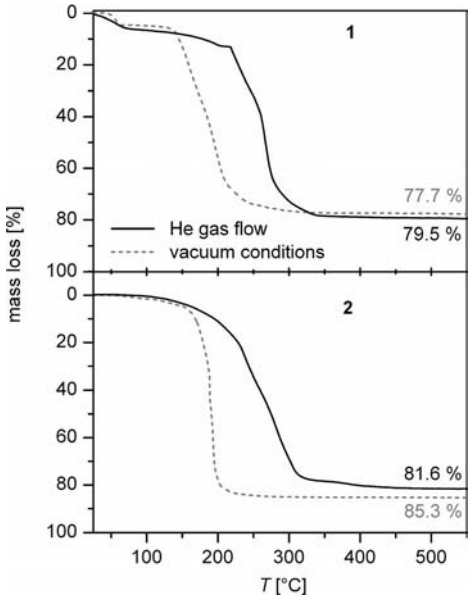

Figure 7. Thermogravimetric analysis of **1** and **2** under He gas flow (straight lines) and under vacuum conditions (dashed lines).

In order to investigate the cleavage products, thermolysis experiments were carried out on a preparative scale (ca. 300 mg) under a N_2 atmosphere (up to 500 °C) in Schlenk tubes located inside a tube furnace (see experimental section for details). Complex **1** visibly starts to decompose at around 200 °C when the black crystals turn grey and a colorless oily liquid forms around the powder. Between 250 and 260 °C, the mixture of solid and liquid material turns red, and more liquid forms, which also condenses in the cool trap. Above 260 °C, the material turns back to black and at 310 °C it was observed to be dry with all yellowish liquid products condensed partly in the tube outside the oven and in the cool trap. ^{1}H and ^{13}C NMR spectra of the collected liquid products reveal that the main cleavage products are SPh_2,[41,42] 15-crown-5 ether, and THF. Additional minor peaks in the alkyl and aryl region of the spectra indicate the formation of side products. Among those most dominant is a multiplet in the ^{1}H spectrum around at 3 ppm (≈ 10% of the total amount of –SPh protons). PhSSPh as a possible product of oxidation was not identified. Therefore, it can be suggested that most probably THF is cleaved in the first step in the TGA of **1** (exp. 6%, calcd. 8.8%), and 4 equiv. of SPh_2 with 2 equiv. of 15-crown-5 (exp. 75.6 calcd. 72%) are simultaneously cleaved in the second step according to Scheme 2.

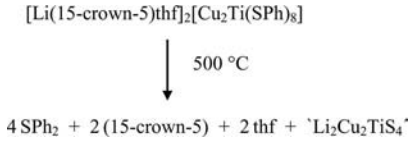

Scheme 2.

The formation of SR_2 and metal sulfides is a well established decomposition pathway for transition metal thiolates $M(SR)_2$ of group 12 (M = Zn, Cd),[43] whereas for binary titanium thiolato complexes different reaction products have been observed. For $Ti(StBu)_4$ either the formation $StBu_2$ and *t*BuSS*t*Bu[3] or formation of H_2S, *t*BuSH and $CH_2{=}C(CH_3)_2$[6] have been reported, and thermolysis of $[NH_2Et_2]_2[Ti_2(SCH_2Ph)_9]$ resulted in the volatile decomposition products Et_2NH and $PhCH_2SSCH_2Ph$.[7]

Complex **2** visibly starts to decompose at around 150 °C with the formation of a dark powder and a colorless oil, which condenses outside the oven. Upon further heating the color of the volatile cleavage products gradually changes to dark yellow. Above 250 °C the cleavage products again appear to be colorless. After cooling, most of the cleavage products outside the oven solidified to result in off-white crystals and a yellow oil. From identification by ^{1}H, ^{13}C, and ^{31}P NMR the main cleavage products are SPh_2 and PPh_3 with traces of $SPPh_3$ and $OPPh_3$ (Scheme 3).

Powder patterns of the residues of the thermal treatment of **1** and **2** up to 500 °C show distinctly different results (Figure 8). Most of the diffraction peaks of the residue of the thermolysis of **1** can be explained by comparison with the peak patterns of $Cu_{1.8}S$ (Digenite) and $Cu_{1.96}S$ (Djurleit).[44] We could not identify peaks corresponding to

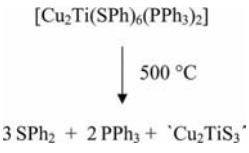

Scheme 3.

known ternary and quaternary phases composed of Cu, Ti, S and Li. In this respect, it is interesting to note that titanium sulfide films produced by CVD processes with substrate temperatures below 800 °C are usually found to be amorphous.[3,6–8] In addition, we found that the positions of the broad peaks (marked by an asterix) are similar to

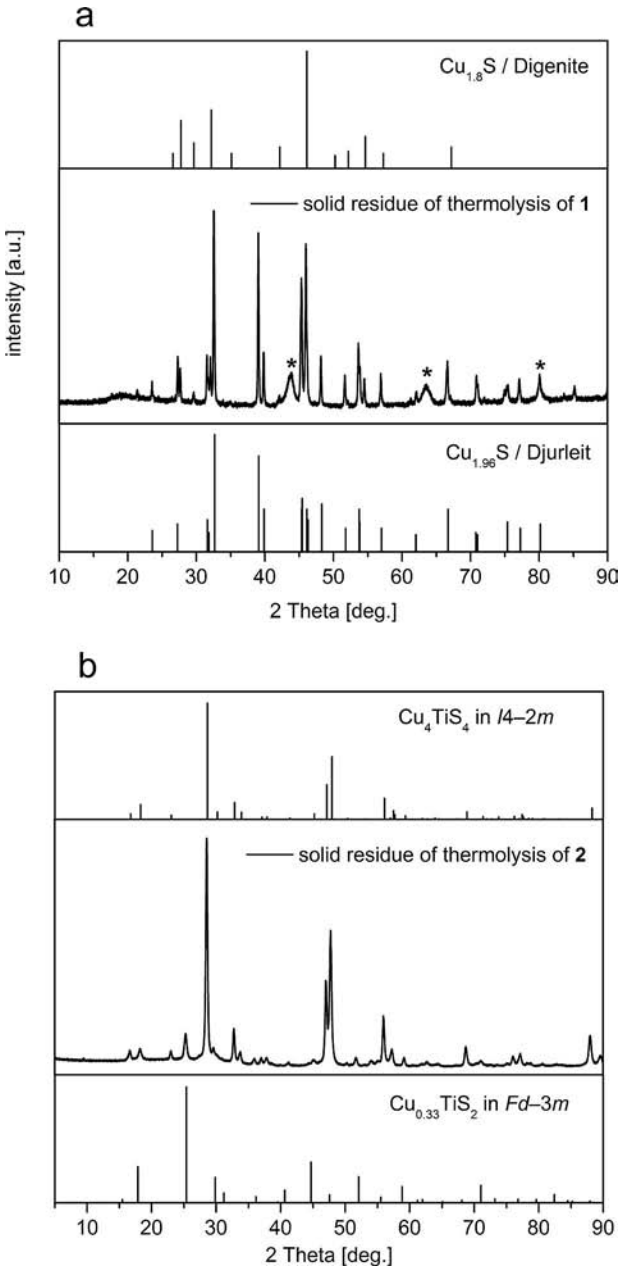

Figure 8. Powder XRD pattern of the residues of the thermolysis (500 °C) of **1** and **2** under nitrogen.

those reported for some $LiTiO_2$ phases.[45,46] However, this would require reduction of Ti^{4+} to Ti^{3+} and the presence of distinct amounts of moisture and the presence of oxygen should also lead to the formation of PhSSPh which was not found in the cleavage products.

In contrast, almost all of the peaks in the diffractogram of the residue of the thermolysis of **2** can be assigned to a mixture of two phases, namely Cu_4TiS_4[47] and the defect thiospinel $Cu_{0.33}TiS_2$.[48] Reflection peak maxima were found to be by five times more intense for Cu_4TiS_4. It is not clear whether this reflects the ratio of the two phases. In addition the formation of $Cu_{0.33}TiS_2$ requires the partial reduction of Ti^{4+} ions to Ti^{3+}. Interestingly, parts of the pattern do not exactly match that of $Cu_{0.07}TiS_2$,[49] which would be more understandable on basis of the formal decomposition Scheme 4.

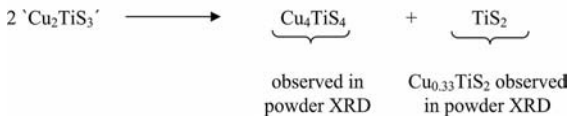

Scheme 4.

TGA experiments under vacuum conditions reveal that **1** and **2** are not suitable for CVD experiments as they decompose before sublimation. However, the ligands are cleaved at temperatures approximately 100 °C lower than under He gas flow. Differences in the total mass loss in comparison with the TGA under He conditions indicate different reaction mechanisms, which were not further investigated.

Conclusions

In conclusion the new homoleptic mixed titanium(IV)/copper(I) trinuclear thiolate complexes $[Li(15\text{-crown-5})thf]_2[Cu_2Ti(SPh)_8]$ and $[Cu_2Ti(SPh)_6(PPh_3)_2]$ have been synthesized in good yields and structurally characterized by single crystal XRD. Density functional calculations reveal that lowest energy transitions in the UV/Vis spectra of both compounds originate from orbitals which are mainly delocalised over the copper and sulfur atoms into orbitals that are essentially localised at the titanium atoms. The calculations also show that additional antibinding π donor interactions of the lone pair *p* orbitals at the terminal sulfur atoms with *d* orbitals at the copper atoms increases the HOMO in $[Li(15\text{-crown-5})thf]_2[Cu_2Ti(SPh)_8]$ resulting in a redshift of the lowest energy absorptions compared to $[Cu_2Ti(SPh)_6(PPh_3)_2]$. Neither compound is well suited to be a precursor for the synthesis of solid state phases. Whereas thermolysis of $[Cu_2Ti(SPh)_6(PPh_3)_2]$ at 500 °C resulted in the formation of a mixture of the two ternary sulfides $Cu_{0.33}TiS_2$ and Cu_4TiS_4, reflections of the powder diffraction patterns of the residues of the thermal analysis of $[Li(15\text{-crown-5})thf]_2[Cu_2Ti(SPh)_8]$ could only be assigned to the known phases $Cu_{1.8}S$ (Digenite) and $Cu_{1.96}S$ (Djurleit). In addition, both complexes were found to decompose under vacuum conditions before sublimation.

Experimental Section

Synthesis: Standard Schlenk techniques were employed throughout the syntheses using a double manifold vacuum line (10^{-3} mbar) with high purity nitrogen (99.99990%). The solvent THF was dried with sodium benzophenone and distilled under nitrogen. Anhydrous CH_3CN ($H_2O < 0.001\%$), CH_2Cl_2 ($H_2O < 0.001\%$), and DMF ($H_2O < 0.005\%$) were obtained from Aldrich and degassed, freshly distilled, and stored over molecular sieves under nitrogen. $TiCl_4{\cdot}2thf$[50] and LiSPh[51] were prepared according to literature procedures. CuCl was washed with HCl, CH_3OH, and diethyl ether to remove traces of $CuCl_2$, then dried under vacuum.

$[Li(15\text{-crown-5})thf]_2[TiCu_2(SPh)_8]$ (1): A solution of PhSLi (700 mg, 6 mmol) in THF (20 mL) was slowly added to a yellow suspension of $TiCl_4{\cdot}2thf$ (250 mg, 0.75 mmol) and CuCl (150 mg, 1.5 mmol) in THF (20 mL). The reaction mixture immediately became dark lilac and was stirred until the CuCl was completely dissolved. After addition of 15-crown-5 (0.3 mL, 1.5 mmol) at –15 °C and stirring for 1 h a dark oil was formed. Careful warming of the reaction mixture to 5–10 °C (ca. 4 h) resulted in the dissolution of the oil followed by the immediate crystallization of black **1**; yield 1020 mg (83%). Crushed fragments of the crystals appear dark green. Complex **1** is partially soluble in thf (21 mg in 10 mL) but after several minutes a yellow precipitate is formed indicating decomposition of **1**. Similar behavior was observed in CH_3CN and CH_2Cl_2. In DMF **1** dissolves to give a red–brown solution, which becomes colorless after 15–20 min. $C_{76}H_{88}Cu_2Li_2O_{12}S_8Ti$ (1646.94): calcd. C 55.4, H 5.9, S 15.6; found C 55.4, H 5.8, S 15.9.

$[Cu_2Ti(SPh)_6(PPh_3)_2]$ (2): Addition of THF (10 mL) to a mixture of $TiCl_4{\cdot}2thf$ (125 mg, 0.375 mmol) and CuCl (95 mg, 0.95 mmol) results in the formation of a yellow suspension. Upon addition of a solution of LiSPh (350 mg, 3 mmol) dissolved in THF (20 mL) the reaction mixture immediately becomes dark lilac. After stirring for 1–2 h, a solution of PPh_3 (400 mg, 1.525 mmol) in THF (20 mL) was added. The reaction mixture immediately became dark blue–gray and after several minutes almost black crystals of **2** started to crystallize to yield after 2 h a total of 460 mg (91%) of **2**. Crystals of **2** are insoluble in THF, CH_3CN, CH_2Cl_2, and DMF at room temp., and gentle heating resulted in the decomposition of **2** indicated by the formation of a yellowish precipitate. $C_{72}H_{60}Cu_2P_2S_6Ti$ (1354.54): calcd. C 63.8, H 4.5, S 14.2; found C 63.8, H 5.1, S 13.5.

Thermolysis: Thermolysis experiments were carried out using a Linn High Term FRHT-70/500/1100 programmable tube furnace, 70 cm long and 4 cm in diameter, equipped with a ca. 50 × 3 cm borosilicate Schlenk tube. For thermolysis under nitrogen the tube with the cool trap was connected by Viton tubing to a mercury bubbler of a Schlenk line. The samples to be pyrolysed were placed in either quartz or porcelain boats in the center of the furnace (ca. 300 mg). The oven was programmed to ramp at a rate of 2 °C/min to 500 °C under a static pressure of N_2 and hold at this temperature for 1 h before cooling to room temperature. The solid residues in the porcelain or quartz boats were characterized by powder X-ray analysis, and the volatile cleavage products deposited in the part of the tube outside the furnace and in the cool trap were collected for ^1H, ^{13}C, and ^{31}P NMR spectroscopy.

Crystallography: Crystals suitable for single-crystal X-ray diffraction were taken directly from the reaction solutions and then coated in perfluoroalkyl ether oil. Single-crystal X-ray diffraction data for **1** and **2** were collected by using graphite-monochromatised Mo-K_α radiation (λ = 0.71073 Å) with a STOE IPDS II (Imaging Plate Diffraction System). Raw intensity data were collected and treated

with the STOE X-Area software, version 1.39. Data for all compounds were corrected for Lorentz and polarisation effects (Table 4).

Table 4. Crystallographic data for **1** and **2**.

	1	**2**[a]
Formula mass [g/mol]	1646.87	1354.48[a]
Crystal system	monoclinic	trigonal
Space group	*P*2(1)/*c*	*R*3
Cell		
a [Å]	12.701(3)	13.6687(19)
b [Å]	19.492(4)	
c [Å]	15.842(3)	31.405(6)
β [°]	94.39(3)	
V [Å^3]	3910.6(14)	5081.4(14)
Z	2	3
T [K]	180	180
$d_{calcd.}$ [g cm^{-3}]	1.399	1.328
$\mu(\lambda)$ [mm^{-1}]	0.911	1.009
F[000]	1724	2094
$2\theta_{max}$ [°]	49	51
Measured reflections	23956	10500
Unique reflections	6553	4234
R_{int}	0.0863	0.0647
Reflections with $I > 2\sigma(I)$	5878	2859
Refined parameters	617	107
*R*1 [$I > 2\sigma(I)$][b]	0.034	0.0590
*wR*2 (all data)[c]	0.0942	0.1457
Abs. structure parameters	–	0.46(6)

[a] Complex **2** crystallizes with approximately 0.5 THF solvent molecules which could not be refined properly because they are localized on a threefold axis. [b] $R1 = \Sigma||F_o| - |F_c||/\Sigma|F_o|$. [c] $wR2 = \{\Sigma[w(F_o^2 - F_c^2)^2]/\Sigma[w(F_o^2)^2]\}^{1/2}$.

Based on a crystal description numerical absorption corrections were applied for **1** and **2**.[52] The structures were solved with the direct methods program SHELXS of the SHELXTL PC suite programs,[53] and were refined with the use of the full-matrix least-squares program SHELXL. Molecular diagrams were prepared using Diamond.[54]

All Cu, Ti, S, P, O, and Li atoms were refined in **1** and **2** with anisotropic displacement parameters, and H atoms were placed in fixed positions. C atoms in **1** were also refined with anisotropic displacement parameters, and all of the phenyl rings in **2** show disorder which was modelled using partial-occupancy carbon atoms constrained into rigid hexagons; these carbons were refined isotropically. Lattice thf molecules were identified within the structure, but these were located on a threefold axis and badly disordered and could not be adequately refined. The data were therefore corrected for these using the SQEEZE option within the PLATON[55] program package finding a total of 69 electrons (ca. 1.5 THF) in a potential solvent accessible area of 299.1 Å. This resulted in improved *R* values [before *R*1 = 0.0634, and *wR*2 (all data) = 0.1586]. The absolute structural parameter (Flack parameter) of 0.48 points to almost perfect racemic twinning. The value of the $|E^2-1|$ statistics (0.864) is between those for acentric and centrosymmetric structures. We therefore tested for missed centrosymmetry. However, refinement in $R\bar{3}$ resulted in *wR*2 values above 0.30 indicating that the centrosymmetry is only fulfilled for the heavy atom structure, indicated by the large correlation matrix elements for the atom pairs Cu1/Cu2, S1/S2, and P1/P2 (0.845, 0.875, and 0.872, respectively) in the final refinement in *R*3. We also attempted to refine in triclinic $P\bar{1}$, with the rhombohedral threefold axis as a twin law, but the refinement proved unstable. In addition, the possibility of merohedral twinning within *R*3 was tested, but the scale factor for this refined to zero. We therefore concluded that the heavily disordered *R*3 structure is correct.

CCDC-808537 (for **1**) and -808538 (for **2**) contain the supplementary crystallographic data for this paper. These data can be obtained free of charge from The Cambridge Crystallographic Data Centre via www.ccdc.cam.ac.uk/data_request/cif.

X-ray powder diffraction patterns for **1** and **2** were measured with a STOE STADI P diffractometer (Cu-$K_{\alpha1}$ radiation, Germanium monochromator, Debye–Scherrer geometry) in sealed glass capillaries and agree with the theoretical powder diffraction patterns calculated on the basis of the atom coordinates obtained from single-crystal X-ray analysis by using the program package STOE WinXPOW.[56]

Quantum Chemical Calculations: Structure optimisations were performed with TURBOMOLE[57,58,59] (v. 6.2) using the BP86[36,37] density functional in combination with def-SV(P)[38] bases and RI-J auxiliary bases[60,61] on all atoms. Orbital analyses and time-dependent DFT calculations were performed with ORCA (v. 2.8.) at the same level of theory. Crystal lattice effects were approximated with COSMO[39] using standard optimised calotte radii, infinite dielectric constant, and a refraction index of 1.4. Further details are given in the Supporting Information.

Physical Measurements: C, H, S elemental analyses were performed with an Elementar vario Micro cube instrument. Solid state UV/Vis spectra were measured on micron sized crystalline powders in mineral oil between quartz plates with a Labsphere integrating sphere. ^{1}H, ^{13}C, and ^{31}P NMR spectra were recorded with a Bruker Avance II 500. Thermogravimetric analyses were run in Al_2O_3 crucibles with a thermobalance STA 409 from Netzsch in a dynamic helium gas flow (25 mL/min) and under vacuum conditions 6×10^{-7} mbar at a heating rate of 2 °C/min. The crucibles were filled (20–35 mg) inside an argon glove box, transferred in Schlenk tubes, and mounted under a stream of argon on the balance. Caution should be taken with respect to the bad smelling volatile products formed in the TGA.

Supporting Information (see footnote on the first page of this article): Tables S1–S8, the 100 lowest energy transitions in **1c**, the 100 lowest energy transitions in **2c**, Cartesian coordinates (Å) of **1c**, Cartesian coordinates (Å) of **2c**, Mulliken-reduced orbital populations per MO in **1c**, Mulliken-reduced orbital populations per MO in **2c**, details of the full gas phase optimisation of $[Cu_2Ti(SPh)_8]^{2-}$ including optimised Cartesian coordinates (Å), details of the full gas phase optimisation of $[Cu_2Ti(SPh)_6(PPh_3)_2]$ including optimised Cartesian coordinates (Å).

Acknowledgments

This work was supported by the Deutsche Forschungsgemeinschaft (DFG) (Center for Functional Nanostructures) and the Karlsruher Institut für Technologie (KIT, Campus Nord). A. E. thanks Dr. Chris Anson for "twin-testing", and the authors are also grateful to E. Tröster, S. Stahl, and N. Metz for their valuable assistance in the practical work.

[1] D. W. Stephan, T. T. Nadasdi, *Coord. Chem. Rev.* **1996**, *147*, 147–208, and references cited therein.
[2] *CVD of Nonmetals* (Ed.: W. S. Rees Jr.,), VCH, Weinheim, Germany, **1996**, 441 pp..
[3] M. Bochmann, I. Hawkins, L. M. Wilson, *J. Chem. Soc., Chem. Commun.* **1988**, 344–345.
[4] C. H. Winter, T. S. Lewkebandara, J. W. Proscia, A. L. Rheingold, *Inorg. Chem.* **1993**, *32*, 3807–3808.

[5] T. S. Lewkebandara, C. H. Winter, *Adv. Mater.* **1994**, *6*, 237–239.
[6] J. Cheon, J. E. Gozum, G. S. Girolami, *Chem. Mater.* **1997**, *9*, 1847–1853.
[7] C. J. Carmalt, C. W. Dinnage, I. P. Parkin, J. W. Steed, *Inorg. Chem.* **2000**, *39*, 2693–2695.
[8] C. J. Carmalt, E. S. Peters, I. P. Parkin, D. A. Tocher, *New J. Chem.* **2005**, *29*, 620–624.
[9] M. S. Whittingham, *Science* **1976**, *192*, 1126–1127.
[10] M. S. Whittingham, *Prog. Solid State Chem.* **1978**, *12*, 41–99.
[11] G. A. Sigel, P. P. Power, *Inorg. Chem.* **1987**, *26*, 2819–2822.
[12] W. Stüer, K. Kirschbaum, D. M. Giolando, *Angew. Chem.* **1994**, *106*, 2028; *Angew. Chem. Int. Ed. Engl.* **1994**, *33*, 1981–1982.
[13] D. T. Corwin Jr., J. F. Corning, S. A. Koch, M. Millar, *Inorg. Chim. Acta* **1995**, *229*, 335–342.
[14] J. T. Kim, J. W. Park, S. M. Koo, *Polyhedron* **2000**, *19*, 1139–1143.
[15] C. Puke, K. Schmengler, K. Kirschbaum, O. Conrad, D. M. Giolando, *Acta Crystallogr., Sect. C* **2000**, *56*, e542.
[16] N. Wheatley, P. Kalck, *Chem. Rev.* **1999**, *99*, 3379–3419.
[17] D. W. Stephan, *Coord. Chem. Rev.* **1989**, *95*, 41–107.
[18] G. S. White, D. W. Stephan, *Organometallics* **1987**, *6*, 2169–2175.
[19] T. A. Wark, D. W. Stephan, *Inorg. Chem.* **1987**, *26*, 363–369.
[20] T. Amemiya, S. Kuwata, M. Hidai, *Chem. Commun.* **1999**, 711–712.
[21] H. Sommer, N. Drebov, A. Eichhöfer, R. Ahlrichs, D. Fenske, *Eur. J. Inorg. Chem.* **2009**, 4329–4334.
[22] V. Bodenez, L. Dupont, M. Morcette, C. Surcin, D. W. Murphy, J.-M. Tarascon, *Chem. Mater.* **2006**, *18*, 4278–4287.
[23] A. C. W. James, J. B. Goodenough, *J. Solid State Chem.* **1988**, *77*, 356–365.
[24] A. H. Reshak, *J. Phys. Chem. A* **2009**, *113*, 1635–1645.
[25] B. K. Maiti, K. Pal, S. Sarkar, *Eur. J. Inorg. Chem.* **2007**, 5548–5555.
[26] J. M. Ball, P. M. Boorman, J. F. Fait, T. Ziegler, *J. Chem. Soc., Chem. Commun.* **1989**, 722–723.
[27] P. C. Leverd, M. Lance, M. Nierlich, J. Vigner, M. Ephritikhine, *J. Chem. Soc., Dalton Trans.* **1994**, 3563–3567.
[28] P. M. Boorman, H. B. Kraatz, M. Parvez, T. Ziegler, *J. Chem. Soc., Dalton Trans.* **1993**, 433–439.
[29] L.-S. Wang, T.-L. Sheng, X. Wang, D.-B. Chen, S.-M. Hu, R.-B. Fu, S.-C. Xiang, X.-T. Wu, *Inorg. Chem.* **2008**, *47*, 4054–4059.
[30] T. Glaser, E. Bill, T. Weyhermuller, W. Meyer-Klaucke, K. Wieghardt, *Inorg. Chem.* **1999**, *38*, 2632–2642.
[31] C. D. Garner, J. R. Nicholson, W. Clegg, *Inorg. Chem.* **1984**, *23*, 2148–2150.
[32] J. R. Nicholson, J. R. Nicholson, W. Clegg, C. D. Garner, *Inorg. Chem.* **1985**, *24*, 1092–1096.
[33] B. K. Maiti, K. Pal, S. Sarkar, *Eur. J. Inorg. Chem.* **2007**, 5548–5555.
[34] R. N. Mukherjee, Ch. Pulla Rao, R. H. Holm, *Inorg. Chem.* **1986**, *25*, 2979–2989.
[35] P. S. Braterman, V. A. Wilson, *J. Organomet. Chem.* **1971**, *26–33*, 131–135.
[36] A. D. Becke, *J. Chem. Phys.* **1993**, *98*, 5648–5652.
[37] J. P. Perdew, *Phys. Rev. B* **1986**, *33*, 8822–8824.
[38] A. Schaefer, H. Horn, R. Ahlrichs, *J. Chem. Phys.* **1992**, *97*, 2571–2577.
[39] a) A. Klamt, *J. Chem. Phys.* **1995**, *103*, 9312–9320; b) A. Schäfer, A. Klamt, D. Sattel, J. C. W. Lohrenz, F. Eckert, *Phys. Chem. Chem. Phys.* **2000**, *2*, 2187–2193.
[40] R. Mulliken, *J. Chem. Phys.* **1955**, *23*, 1833–1840.
[41] S. Perumal, R. Chandrasekaran, V. Vijayabaskar, D. A. Wilson, *Magn. Reson. Chem.* **1995**, *33*, 779–90.
[42] S.-K. Chung, K. Sasamoto, *J. Org. Chem.* **1981**, *46*, 4590–4592.
[43] M. Bochmann, *Chem. Vap. Deposition* **1996**, *2*, 85–96.
[44] A. Janosi, *Acta Crystallogr.* **1964**, *17*, 311–312.
[45] T. Hewston, B. Chamberland, *J. Phys. Chem. Solids* **1987**, *48*, 97–108.
[46] A. Lecerf, *Ann. Chim. (Paris).* **1962**, *7*, 513.
[47] K. O. Klepp, D. Gurtner, *J. Alloys Compd.* **1996**, *243*, 19–22.
[48] T. Kusawake, Y. Takahashi, M. Y. Wey, K. I. Ohshima, *J. Phys. Condens. Matter* **2001**, *13*, 9913–9921.
[49] A. C. W. P. James, J. B. Goodenough, N. J. Clayden, P. M. Banks, *Mat. Res. Bull.* **1989**, *24*, 143–155.
[50] L. E. Manzer, *Inorg. Synth.* **1982**, *21*, 135–140.
[51] R. Köster, G. Seidel, R. Boese, *Chem. Ber.* **1988**, *121*, 1137–1142.
[52] *X-RED32*, v. 1.01, data reduction program, Stoe & Cie GmbH, Darmstadt, Germany, **2001**.
[53] G. M. Sheldrick, *SHELXTL*, PC version 5.1, *An Integrated System for Solving, Refining, and Displaying Crystal Structures from Diffraction Data*, Bruker Analytical X-ray Systems, Karlsruhe, Germany, **2000**.
[54] K. Brandenburg, *Diamond*, version 2.1d, Crystal Impact GbR, 1996–**2000**.
[55] A. L. Spek, *Acta Cryst. Sect. A* **1990**, *46*, C-34.
[56] STOE, *WinXPOW*, STOE & Cie GmbH, Darmstadt, Germany, **2000**.
[57] R. Ahlrichs, M. Bär, M. Häser, H. Horn, C. Kölmel, *Chem. Phys. Lett.* **1989**, *162*, 165–169.
[58] O. Treutler, R. Ahlrichs, *J. Chem. Phys.* **1995**, *102*, 346–354.
[59] M. von Arnim, R. Ahlrichs, *J. Chem. Phys.* **1999**, *111*, 9183–9190.
[60] K. Eichkorn, O. Treutler, H. Ohm, M. Häser, R. Ahlrichs, *Chem. Phys. Lett.* **1995**, *240*, 283–289.
[61] K. Eichkorn, F. Weigend, O. Treutler, R. Ahlrichs, *Theor. Chim. Acta* **1997**, *97*, 119–124.

Received: February 8, 2011
Published Online: June 15, 2011

